A Computation of Potential Vorticity Dynamics for Small Rossby Number 2D Rotating Shallow Water

Colin Macdonald, Alana McKenzie

(APMA 930 – Final Project)

Abstract— **Vorticity dynamics resulting from the shallow water equations are investigated for specific potentials, which prevent the formation of gravity waves. We consider only the small Rossby number case, and solve asymptotically to leading order and first correction. Spectral methods are applied to this problem, and the implementation and arising complications are discussed. Resulting vorticity fields exhibit the formation of coherent structures, which parallels previous studies of the shallow water system.**

Index Terms—**rotating shallow water, spectral methods, asymptotics.**

I. INTRODUCTION

THE 2D rotating shallow water equations (rSW) form one of the systems used to model mesoscale dynamics in the ocean and the atmosphere. In 1994, Polvani et al ([1]) analyzed solutions to rSW for various Rossby ($\mathcal{R}$) and Froude ($\mathcal{F}$) numbers, without making any asymptotic assumptions limiting their sizes as the system evolves. Polvani et al ([1]) take care to ensure gravity waves do not affect the long-term solution, and consider the sensitivity of gravity wave formation on the numerical method. Studies of the vorticity field evolution shows the development of coherent structures, which leads to a break down in symmetry between cyclones and anticyclones from random and symmetric initial conditions, ([1]). In particular, Polvani et al ([1]) notes greater anticyclonic preference with larger Froude number.

In our study, we circumvent the numerical dependence of gravity wave formation by restricting velocity and height measures to specific potentials, which eliminates the possibility of gravity wave formation. We only consider the case where $\mathcal{F} = Ro$, for small Rossby number. Assuming Ro remains small as the system evolves, we consider an asymptotic expansion in Ro. The choice of potentials enables the system to reduce nicely in the leading order and first correction.

Our aim for this project is to implement a numerical scheme to analyze vorticity evolution in rSW for the particular potentials. We outline the algorithm used, and discuss the complications that arise in the computational scheme. We qualitatively compare our results to Polvani et al and Hakim et al ([2]), which show coherent structure formation.

II. THE EQUATIONS

Consider the two-dimensional rotating shallow water equations

$$\frac{\mathrm{D}u}{\mathrm{D}t} - fv = -g\frac{\partial h}{\partial x}, \tag{1a}$$

$$\frac{\mathrm{D}v}{\mathrm{D}t} + fu = -g\frac{\partial h}{\partial y}, \tag{1b}$$

$$\frac{\partial h}{\partial t} + \frac{\partial hu}{\partial x} + \frac{\partial hv}{\partial y} = 0, \tag{1c}$$

where u and v are the horizontal velocities, h is the fluid height, f is the Coriolis parameter, and g is the gravitational constant. These equations, after scaling and nondimensionalizing become

$$\mathcal{R}\frac{\mathrm{D}u}{\mathrm{D}t} - v = -h_x, \tag{2a}$$

$$\mathcal{R}\frac{\mathrm{D}v}{\mathrm{D}t} + u = -h_y, \tag{2b}$$

$$\mathcal{R}\frac{\mathrm{D}h}{\mathrm{D}t} + (1 + \mathcal{R}h)(u_x + v_y) = 0, \tag{2c}$$

where $\mathcal{R} = \frac{\text{advection effects}}{\text{Coriolis effects}} = \frac{U}{fL} < 1$. From (2) we can derive the potential vorticity relations

$$\frac{\mathrm{D}q}{\mathrm{D}t} = 0, \tag{3a}$$

$$1 + \mathcal{R}q = \frac{1 + \mathcal{R}(v_x - u_y)}{1 + \mathcal{R}h}. \tag{3b}$$

If we substitute the potentials

$$u = -H_y - F, \tag{4a}$$

$$v = H_x - G, \tag{4b}$$

$$h = G_x - F_y + H, \tag{4c}$$

([3], and see also [4]) into (2) the following system results:

$$\nabla^2 G - G = \mathcal{R}\left(\left[\frac{\mathrm{D}h}{\mathrm{D}t} + h(u_x + v_x)\right]_y + \frac{\mathrm{D}u}{\mathrm{D}t}\right), \tag{5a}$$

$$-(\nabla^2 F - F) = \mathcal{R}\left(\left[-\frac{\mathrm{D}h}{\mathrm{D}t} + h(u_x + v_x)\right]_x + \frac{\mathrm{D}v}{\mathrm{D}t}\right), \tag{5b}$$

$$q - (\nabla^2 H - H) = \mathcal{R}(-qh) + \mathcal{O}(\mathcal{R}^2), \tag{5c}$$

$$\frac{\mathrm{D}q}{\mathrm{D}t} = 0. \tag{5d}$$

Note that although (5) seems to have many time derivatives, most cancel out in the leading-order and first-correction leaving only a advective derivative on q; this is one of the

reasons why this is a particularly convenient formulation for computation.

First we consider the leading order (zero-Rossby number) or *Quasi-Geostrophic* (QG) case where (5) reduces to

$$\nabla^2 G_0 - G_0 = 0, \tag{6a}$$

$$\nabla^2 F_0 - F_0 = 0, \tag{6b}$$

$$\nabla^2 H_0 - H_0 = -q, \tag{6c}$$

$$\frac{Dq}{Dt} = 0. \tag{6d}$$

On a periodic domain (as we will consider for our numerical experiments), (6a) and (6b) imply $G_0 = 0$ and $F_0 = 0$.[1] The remaining two equations suggest the following algorithm for time-stepping the dynamics of q for the Quasi-Geostraphy case:

1) given q
2) solve (6c) for H_0
3) compute $u = u_0 = -H_{0y}$, $v = v_0 = H_{0x}$.
4) use u and v to advect q.
5) repeat using new q.

Note that the operator $\nabla^2 - 1$ is particularly well-behaved (compared to, say $\nabla^2 + 1$) for its eigenvalues are never zero.

A. First-Correction

The leading-order results tell us that the asymptotic expansions for F, G and H are

$$F = 0 + \mathcal{R}F_1,$$
$$G = 0 + \mathcal{R}G_1,$$
$$H = H_0 + \mathcal{R}H_1,$$

and substituting back in (5) gives us the equations for the first-correction:

$$\nabla^2 G_1 - G_1 = H_{0y}H_{0yx} - H_{0x}H_{0yy}$$
$$= -J(H_0, H_{0y}), \tag{8a}$$

$$\nabla^2 F_1 - F_1 = H_{0y}H_{0xx} - H_{0x}H_{0xy}$$
$$= -J(H_0, H_{0x}), \tag{8b}$$

$$\nabla^2 H_1 - H_1 = qH_0, \tag{8c}$$

$$\frac{Dq}{Dt} = 0. \tag{8d}$$

Note that the equations for G_1, F_1, and H_1 all involve the same $\nabla^2 - 1$ operator as the H_0 equation from the leading order. We thus consider the following algorithm for computing the leading-order small-Rossby number dynamics of the potential vorticity q:

1) given q
2) solve (6c) for H_0
3) solve (8a), (8b) and (8c) for G_1, F_1 and H_1
4) compute:

$$u = u_0 + \mathcal{R}u_1 = -\frac{\partial}{\partial y}(H_0 + \mathcal{R}H_1) - \mathcal{R}F_1,$$

$$v = v_0 + \mathcal{R}v_1 = \frac{\partial}{\partial x}(H_0 + \mathcal{R}H_1) - \mathcal{R}G_1.$$

[1]To see this, consider the 1D equation $\nabla^2 G - G = 0$ with general solution of the form $G = Ae^{\pm x}$ and note only $A = 0$ satisfies the boundary conditions.

5) use u and v to advect q.
6) repeat using new q.

III. IMPLEMENTATION

The algorithms outlined above are implemented using spectral methods (see for example [5]). We consider the unit square domain with periodic boundary conditions using a uniform discretization of $N_x \times N_y$ points.

A. Initial Conditions

We generate our initial conditions in the frequency domain by assigning random amplitudes for any mode which satisfies $k_1 \leq ||\boldsymbol{k}||_2 \leq k_2$ for choosen values of k_1 and k_2. This assigns energy to a "ring" of wave numbers. We then compute the IFFT of these conditions to produce initial conditions in the spatial domain which consist of random waves of scales ranging from k_1 to k_2.

B. Time-stepping

For advecting q we use second-order Adams-Bashforth:

$$u^{n+1} = u^n + \frac{3}{2}\Delta t f(u^n) - \frac{1}{2}\Delta t f(u^{n-1}) \tag{9}$$

Since this method is not self starting, we use 20 small steps of Forward Euler to get to $t = t_1 = \Delta t$.

C. De-aliasing

Functions in the spectral domain are characterized by their frequency mode, k. Discretizing x in the physical domain limits the number of modes in the frequency domain, and the number of allowed modes is inversely proportional to the grid spacing. For a function sampled at intervals Δx in physical space, we must ensure that the grid spacing is small enough to allow for enough modes to characterize the function. Otherwise the high frequency modes are mapped to lower frequency modes, which is known as aliasing.

An example of aliasing can be seen in Figure 1. Shown are plots of $\cos 2x$ and $\frac{1}{2} + \frac{1}{2}\cos 4x$, and the values of both functions at intervals $\Delta x = \frac{\pi}{3}$. From only the function values along grid points, the two functions are indistinguishable. Aliasing occurs in cases like this, when a higher frequency mode appears as a lower frequency mode.

Aliasing is does not present a significant problem in terms of initial conditions, since an appropriate grid size can be selected (at the so-called *Nyquist rate*). Where aliasing becomes an issue however, is in multiplying two or more well-sampled terms.

Consider another example, this time of $\cos 2x \cos 2x$. While a grid size of $\Delta x = \frac{\pi}{3}$ properly resolves $\cos 2x$, the product $\cos 2x \cos 2x = \frac{1}{2} + \frac{1}{2}\cos 4x$ is affected by aliasing. The higher mode, $\cos 4x$ is mapped to a lower mode, $\cos 2x$ (as seen in Figure 1).
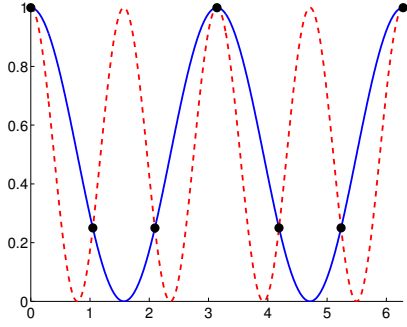
Fig. 1.   An example of aliasing: sampling these two functions on an grid with spacing $\frac{\pi}{3}$ results in the same discrete signal.

Fig. 2.   Spectum plots for QG, $N = 128$, for various artificial diffusion terms. No artificial diffusion (top-left); 2$^{\text{nd}}$-order diffusion, $\mu = 1 \times 10^{-5}$ (top-right); 8$^{\text{th}}$-order diffusion, $\mu = 10^{-15}$ (bottom-left); 8$^{\text{th}}$-order diffusion, $\mu = 10^{-19}$ (bottom-right). In each case, the solid vertical line indicates the grid scale.

In general, multiplication in physical space is equivalent to convolution in frequency space, and can be written as:

$$
\begin{aligned}
u_j v_j &= \sum_{k_1=-\frac{N}{2}}^{\frac{N}{2}-1} \widehat{u_{k_1}} e^{\frac{i2\pi}{N}jk_1} \sum_{k_2=-\frac{N}{2}}^{\frac{N}{2}-1} \widehat{v_{k_2}} e^{\frac{i2\pi}{N}jk_2} \\
&= \sum_{k_1=-\frac{N}{2}}^{\frac{N}{2}-1} \sum_{k_2=-\frac{N}{2}}^{\frac{N}{2}-1} \widehat{u_{k_1}} \widehat{v_{k_2}} e^{\frac{i2\pi}{N}j(k_1+k_2)}
\end{aligned} \tag{10}
$$

Therefore, when u and v are discretized to N modes, their product contains $2N$ modes. Furthermore,

$$
e^{\frac{i2\pi}{N}j(k_1+k_2)} = e^{\frac{i2\pi}{N}j(k_1+k_2+N)} \tag{11}
$$

so modes where $|k_1 + k_2| > \frac{N}{2}$ are aliased to the $k_1 + k_2 - N$ mode.

To resolve this problem, we can anticipate the creation of additional modes when multiplying. By increasing the number of frequency modes prior to multiplication, the computation becomes more expensive, but the higher modes are not aliased. For each multiplication we need to determine how many frequency modes to include, N_2, where $\max(k_1 + k_2) - N_2 > \frac{N}{2}$. In the case of two-term multiplication on equal grids, $N_2 = \frac{3}{2}N$.

This process is known as de-aliasing. To implement de-aliasing, we wrote the function padAndMult, which takes two functions in the frequency domain as inputs, and returns their product in frequency domain without aliased wave modes.

The pseudocode for padAndMult is:

1) given inputs $\hat{a}$ and $\hat{b}$.
2) add $\frac{N}{4}$ zeros to either end of the input functions, for a total of $\frac{3}{2}N$ modes. This is called zero padding.
3) multiply the zero-padded functions. This is done as $\hat{c} = \text{fft}(\text{ifft}(\hat{a})\text{ifft}(\hat{b}))$
4) truncate $\frac{N}{4}$ values from either end of the result, removing the higher frequencies.
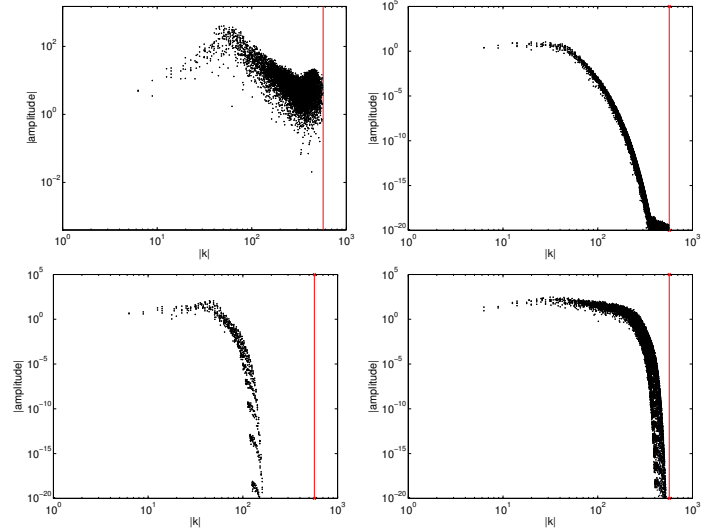5) return the truncated $\hat{c}$

D. Artificial diffusion

We add an artificial diffusion term to (6d) and (8d), replacing them with

$$
\frac{\mathrm{D}q}{\mathrm{D}t} = -\mu(\nabla^2)^4 q. \tag{12}
$$

This helps stabilize our numerical method by damping out high frequency modes that are close to the "grid scale", that is, those that have wavelengths close to Δx or Δy. In the absence of an artificial diffusion term, energy is transferred to these grid scale modes through a *spectral cascade*.

The parameter $\mu > 0$ needs to be chosen so that the damping "turns on" near the grid scale and damps out the appropriate modes without significantly damping features on the smaller (physical) scales. The choice of μ depends on Δx, Δy, and presumably $\mathcal{R}$ in the first correction case.

Figure 2 shows *spectrum* plots of amplitudes versus wave number magnitudes for various artificial diffusion terms.

E. Integrating factor

The introduction of artificial diffusion imposes a strict timestep restriction for explicit methods. Using an *integrating factor*, we alleviate this restriction by incorporating the exact solution to the linear terms. Consider the advection equation with artificial diffusion added.

$$
q_t + uq_x + vq_y = -\mu(\nabla^2)^4 q.
$$

Taking the Fourier transform, we get:

$$
\begin{aligned}
\widehat{q_t} + \widehat{uq_x} + \widehat{vq_y} &= -\mu(\widehat{(\nabla^2)^4 q}), \\
\widehat{q_t} + \widehat{uq_x} + \widehat{vq_y} &= -\mu(k^8 + j^8)\widehat{q}.
\end{aligned}
$$

Since we know the solution to the linear equation, we can reduce the two linear terms to one term by multiplying the

equation by $e^{-\mu(k^8+j^8)t}$:

$$\hat{q}_t e^{-\mu(k^8+j^8)t} - \mu(k^8+j^8)\widehat{q}e^{-\mu(k^8+j^8)t}$$
$$= -(\widehat{uq_x} + \widehat{vq_y})e^{-\mu(k^8+j^8)t},$$
$$(\hat{q}e^{-\mu(k^8+j^8)t})_t = -(\widehat{uq_x} + \widehat{vq_y})e^{-\mu(k^8+j^8)t}.$$

Letting $RHS = -(\widehat{uq_x} + \widehat{vq_y})$ and $m = \mu(k^8+j^8)$, we get:

$$(\hat{q}e^{-mt})_t = RHSe^{-mt}.$$

Solving for $\hat{q}$ using Forward Euler:

$$\widehat{q_{n+1}}e^{-m(t+\Delta t)} = \widehat{q_n}e^{-mt} + \Delta t RHS_n e^{-mt},$$
$$\widehat{q_{n+1}} = \widehat{q_n}e^{m\Delta t} + \Delta t RHS_n e^{m\Delta t},$$

and similarly using Adams-Bashforth

$$\widehat{q_{n+1}} = \widehat{q_n}e^{m\Delta t} + \frac{3\Delta t}{2}\left[RHS_n e^{m\Delta t}\right]$$
$$- \frac{\Delta t}{2}\left[RHS_{n-1}e^{2m\Delta t}\right].$$

We can define the time independent integrating factors: $I_1 = e^{m\Delta t}$ and $I_2 = e^{2m\Delta t}$. These can be computed once initially and stored for use at each timestep.

F. Pseudocode

The pseudo-code for the quasi-geography case is:
1) compute $\widehat{q}$, the FFT of q.
2) solve (6c): $\widehat{H_0} = -\hat{q}/(-1-k^2-l^2)$.
3) compute $\widehat{q_x}$, $\widehat{q_y}$, $\widehat{H_{0x}}$, $\widehat{H_{0y}}$ and $(\widehat{\nabla^2})^4 q$.
4) compute $\hat{u}$ and $\hat{v}$.
5) compute $\widehat{q_x u}$ and $\widehat{q_y v}$ using the de-aliasing `padAndMult` (note this involves FFT and IFFT calls).
6) timestep $\frac{\partial \hat{q}}{\partial t} = -\widehat{q_x u} - \widehat{q_y v} - \mu(\widehat{\nabla^2})^4$ using the integrating factors and Adams-Bashforth to obtain a new $\hat{q}$.
7) return to step 2.

The pseudo-code for the first correction case is:
1) compute $\widehat{q}$, the FFT of q.
2) solve (6c): $\widehat{H_0} = -\hat{q}/(-1-k^2-l^2)$.
3) compute $\widehat{H_{0x}}$, $\widehat{H_{0y}}$ $\widehat{H_{0xx}}$, $\widehat{H_{0yy}}$, $\widehat{H_{0xy}}$, $\widehat{q_x}$, $\widehat{q_y}$, and $(\widehat{\nabla^2})^4 q$.
4) compute the products on the right hand sides of (8a) and (8b) using `padAndMult`.
5) solve (8a), (8b), and (8c) for $\widehat{G_1}$, $\widehat{F_1}$, and $\widehat{H_1}$.
6) compute $\hat{u}$ and $\hat{v}$ from above quantities.
7) compute $\widehat{q_x u}$ and $\widehat{q_y v}$ using `padAndMult`.
8) timestep $\frac{\partial \hat{q}}{\partial t} = -\widehat{q_x u} - \widehat{q_y v} - \mu(\widehat{\nabla^2})^4$ using the integrating factors and Adams-Bashforth to obtain a new $\hat{q}$.
9) return to step 2.

The code are written in `matlab` using `fft2` and `ifft2` for computing the FFTs.

IV. RESULTS

A. Time convergence test

Figure 3 shows the results of a time convergence test. In lieu of an exact solution we compute a solution with much smaller time steps and approximate errors against that. Note that our code appears to be second-order in time.
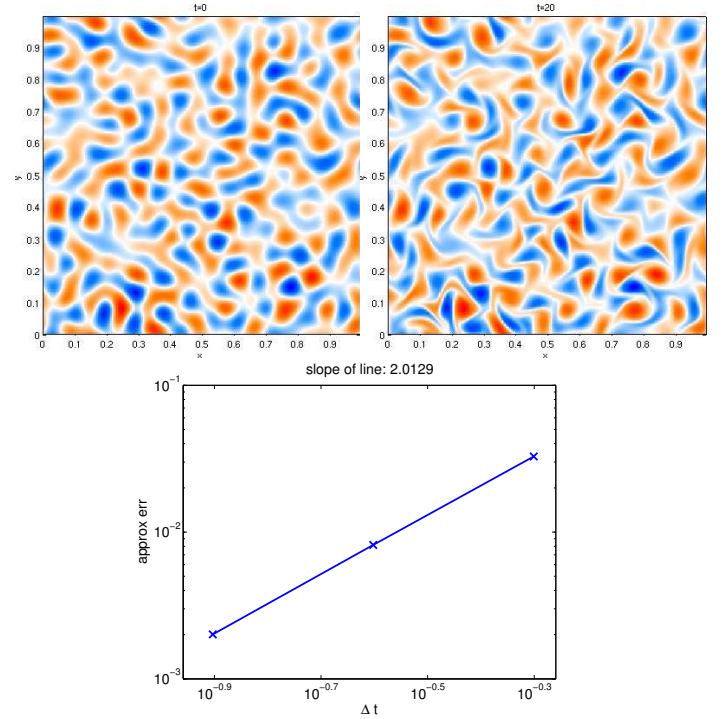

Fig. 3.   Time convergence test. Initial conditions (top-left); Example results at $t = 20$ (top-right); loglog convergence plot (bottom). Error is approximated in the l_2 norm against a solution computed with the smaller stepsize of $\Delta t = .025$.

B. Spatial convergence test

Figure 4 shows two the results of using two different resolutions with the same initial conditions. In case each case, μ is chosen as small as possible while still stabilizing the calculations.

The results appear to be similar but not identical; this suggests that modes near grid scale in the $N = 256$ case may contribute to the dynamics for these initial conditions. A computation with $N = 1024$ should be performed to see if the $N = 512$ computation is sufficiently resolved.

C. QG and first correction comparison

Figure 5 shows the results of running both the QG and the first correction code with $\mathcal{R} = 0.2$ until $t = 1000$. For small times the results appear almost identical but at $t = 1000$ the results, while showing similar features, are not identical. In both the QG and first correction cases, we note, as in [2] and [1], the formation of coherent structures.

V. CONCLUSIONS AND FUTURE WORK

We have successfully implemented a spectral code to compute the vorticity dynamics of the shallow water equations to leading order and small Rossby first correction. The code produces vorticity dynamics which appear consistent with previous results, particularly in the development of coherent structures.

One possible application of this code is to investigate the breakdown in symmetry between cyclones and anticyclones between statistically symmetric initial conditions (as seen in

[2] for the density stratified case). This will require careful exploration of initial conditions and parameters.

REFERENCES

[1] L. M. Polvani, J. C. McWilliams, M. A. Spall, and R. Ford, "The coherent structures of shallow-water turbulence: Deformation-radius effects, cyclone/anticyclone asymmetry and gravity-wave generation," *Chaos: An Interdisciplinary Journal of Nonlinear Science*, vol. 4, no. 2, pp. 177–186, 1994.

[2] G. J. Hakim, C. Snyder, and D. J. Muraki, "A new surface model for cyclone-anticyclone asymmetry," *J. Atmospheric Sci.*, vol. 59, no. 16, pp. 2405–2420, 2002.

[3] D. J. Muraki, "Notes on rotating shallow water," January 2005, private commuication.

[4] D. J. Muraki, C. Snyder, and R. Rotunno, "The next-order corrections to quasigeostrophic theory," *J. Atmospheric Sci.*, vol. 56, no. 11, pp. 1547–1560, 1999.

[5] L. N. Trefethen, *Spectral methods in MATLAB*, ser. Software, Environments, and Tools. Philadelphia, PA: Society for Industrial and Applied Mathematics (SIAM), 2000.
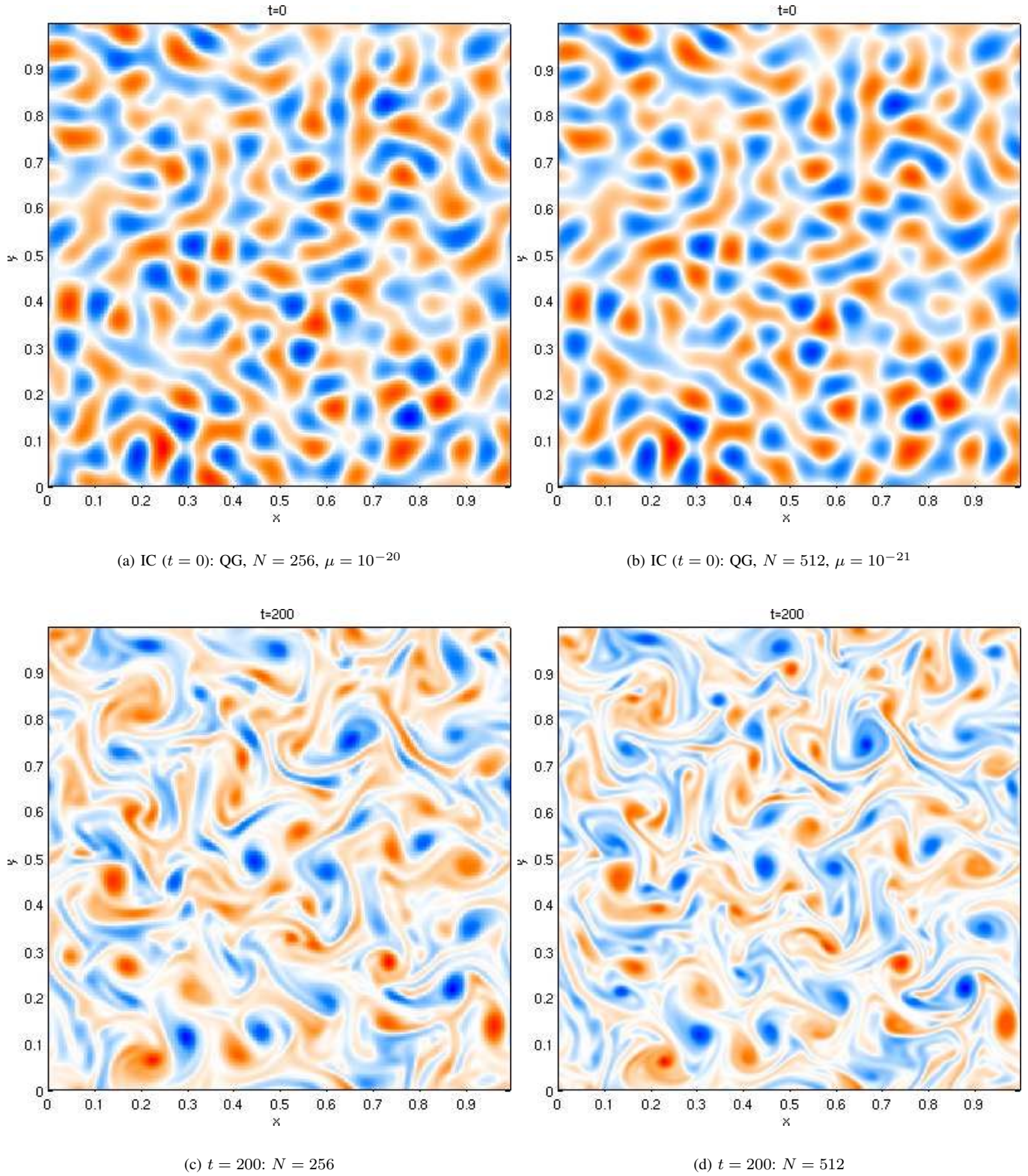
(a) IC ($t = 0$): QG, $N = 256$, $\mu = 10^{-20}$

(b) IC ($t = 0$): QG, $N = 512$, $\mu = 10^{-21}$

(c) $t = 200$: $N = 256$

(d) $t = 200$: $N = 512$

Fig. 4.   Results of spatial convergence test. Note results are fairly similar although not identical.

(a) IC ($t = 0$)

(b) $t = 200$: QG or first correction (results appear similar)

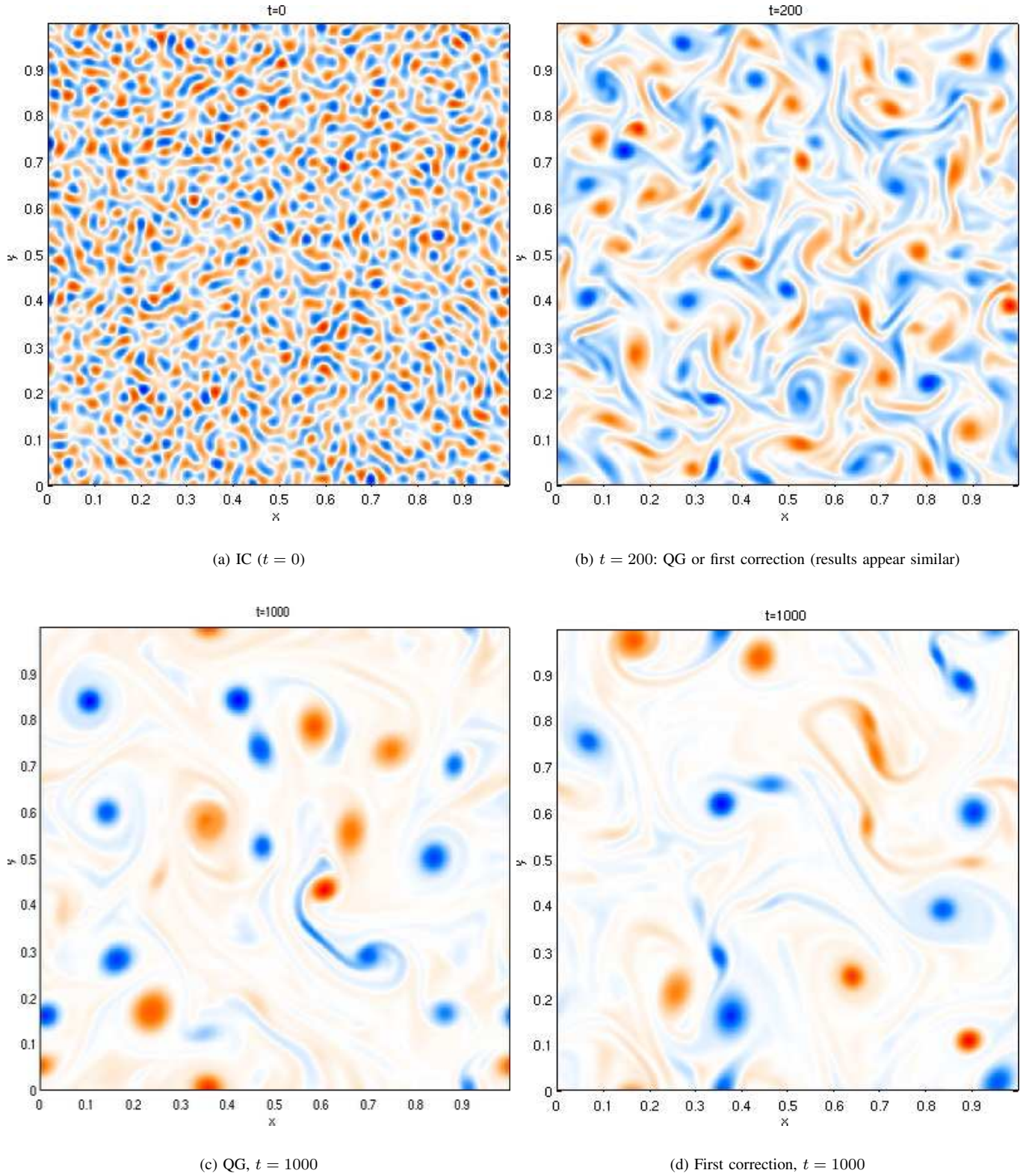(c) QG, $t = 1000$

(d) First correction, $t = 1000$

Fig. 5. Results of QG and first-correction runs for longer times. $N = 512$, $\mathcal{R} = 0.2$.